1-5-2005

A Full-wave Investigation of the Use of a "Cancellation Factor" in Gravity Wave–OH Airglow Interaction Studies

Michael P. Hickey Ph.D.
Embry-Riddle Aeronautical University, hicke0b5@erau.edu

Yonghui Yu
Embry-Riddle Aeronautical University

Scholarly Commons Citation

Hickey, M. P., and Y. Yu (2005), A full-wave investigation of the use of a "cancellation factor" in gravity wave–OH airglow interaction studies, J. Geophys. Res., 110, A01301, doi: https://doi.org/10.1029/2003JA010372.

A full-wave investigation of the use of a "cancellation factor" in gravity wave–OH airglow interaction studies

Michael P. Hickey and Yonghui Yu

Department of Physical Sciences, Embry-Riddle Aeronautical University, Daytona Beach, Florida, USA

Received 23 December 2003; revised 27 July 2004; accepted 17 November 2004; published 5 January 2005.

[1] Atmospheric gravity waves (GWs) perturb minor species involved in the chemical reactions of airglow emissions in the upper mesosphere and lower thermosphere. In order to determine gravity wave fluxes and the forcing effects of gravity waves on the mean state (which are proportional to the square of the wave amplitude), it is essential that the amplitude of airglow brightness fluctuation be related to the amplitude of major gas density fluctuation in a deterministic way. This has been achieved through detailed modeling combining gravity wave dynamics described using a full-wave model with the chemistry relevant to the airglow emission of interest. Alternatively, others have employed approximations allowing them to derive analytic expressions relating airglow brightness fluctuations to major gas density fluctuations through a so-called "cancellation factor" (CF). The effects of these approximations on the derived CF are investigated here using a full-wave model describing gravity wave propagation in a nonisothermal, windy, and viscous atmosphere. This numerical model combined with the chemical reaction scheme for the OH (8, 3) Meinel airglow emission is used to derive fluctuations in the OH* nightglow from which an equivalent CF is calculated. Comparisons are made between the analytically derived CF's and the numerically derived CF's based on using different approximations in the latter model. Differences exist at most wave periods, but they also depend on the horizontal wavelengths of the gravity waves considered. In addition to these different model comparisons, the sensitivity of the numerically derived CF to specific physical processes is examined exclusively using the full-wave model. These sensitivity tests show that the effect of eddy diffusion marginally influences the calculated CF's only for the very slowest gravity waves. Accounting for the effects of a nonisothermal mean state has a significant influence on the calculated CF's, and the CF's calculated assuming an isothermal mean state can be as much as a factor of 2 smaller than those calculated assuming a nonisothermal mean state. The effects of background mean winds also influence the derived CF's, which then become dependent on the azimuth of propagation. In this case the calculated CF's can vary by a factor of $\sim$2 from their windless values for gravity waves of short horizontal wavelength with phase speeds less than 100 m s^{-1}. Finally, reflection from the lower and middle thermosphere in the full-wave model leads to undulations in the calculated CF's as a function of phase speed for gravity waves with horizontal wavelengths of 100 km and phase speeds greater than about 100 m s^{-1}. These effects that are not reproduced in the analytic model lead to large differences between the CF's calculated with and without winds, but they only occur for fast gravity waves that are not usually observed in the airglow.

Citation: Hickey, M. P., and Y. Yu (2005), A full-wave investigation of the use of a ''cancellation factor'' in gravity wave–OH airglow interaction studies, *J. Geophys. Res.*, *110*, A01301, doi:10.1029/2003JA010372.

1. Introduction

[2] It is well recognized that gravity waves propagating in the mesopause region modulate airglow emissions [*Hecht et al.*, 1993, 1994; *Taylor et al.*, 1995; *Swenson et al.*, 1995; *Smith et al.*, 2000] and a significant amount of modeling has been performed to provide a better understanding of the modulation processes [*Walterscheid et al.*, 1987; *Hines and Tarasick*, 1987; *Schubert and Walterscheid*, 1988; *Hickey*, 1988a, 1988b; *Schubert et al.*, 1991; *Makhlouf et al.*, 1995; *Swenson and Liu*, 1998; *Swenson et al.*, 1999; *Walterscheid et al.*, 1999; *Hecht et al.*, 2001; *Hickey and Brown*, 2002; *Tang et al.*, 2002; *Liu and Gardner*, 2004].

0148-0227/05/2003JA010372

Ground-based observations are able to provide useful measures of gravity wave parameters such as the extrinsic wave period, the extrinsic phase speed, the horizontal wavelength, and the direction of propagation [*Swenson et al.*, 1995]. If these optical instruments are colocated with a wind/temperature lidar (for example), then the height variation of mean horizontal winds can be inferred and used to calculate the height-dependent wave intrinsic period [e.g., *Hickey et al.*, 1998]. The wave intrinsic period is one key parameter required to calculate wave fluxes of momentum, energy and sensible heat. Another key parameter required to calculate wave fluxes is the gravity wave amplitude, which in general is also a function of height.

[3] Determining gravity wave amplitudes from airglow observations is not a trivial task for two fundamental reasons. First, the minor species involved in the specific airglow emission chemistry fluctuate in response to a gravity wave so that the airglow fluctuation cannot be easily related to the fluctuation of the major gas. (The individual minor species will all fluctuate with different amplitudes that are usually much greater than the fluctuation in the major gas. Additionally, the height variation of the minor species fluctuations does not exactly follow that of the major gas because chemistry is usually important, which implies that the minor species vertical wavelengths are not equivalent to the gravity wave vertical wavelength.) The second difficulty is due to the fact that the observed airglow brightness (for example, at the ground) constitutes a height integral of the volume emission rate (VER) over the vertical extent of the emission layer ($\sim$10 km). This smears the gravity wave effects in the airglow in a way that tends to favor the observation of the faster, long vertical wavelength gravity waves while making the observation of the short vertical wavelength gravity waves difficult or even impossible [*Hines and Tarasick*, 1987; *Schubert and Walterscheid*, 1988; *Schubert et al.*, 1991; *Swenson and Gardner*, 1998; *Hickey and Walterscheid*, 1999].

[4] Two methods for determining wave amplitudes from airglow measurements have been discussed in the literature. The first uses a full-wave model, described in section 2.2, to calculate the altitude variation of fluctuations in major gas density, temperature, and velocity [*Hickey et al.*, 1997, 1998; *Hickey and Brown*, 2002]. These fluctuations are then used in a set of chemically coupled minor species continuity equations to calculate the minor species response to the gravity wave as a function of height, from which VER fluctuations are derived. These are then integrated over height to provide the airglow brightness fluctuation. The original gravity wave amplitudes used in the model are then re-scaled to provide exact agreement between the modeled and observed relative airglow brightness amplitudes (this can be done because the full-wave model is linear). This provides gravity wave amplitudes and phases as a function of height while simultaneously providing a match to the observed airglow fluctuation parameters. When mean horizontal wind information is available, the altitude variation of the derived gravity wave amplitudes sometimes display complicated structure around critical levels [*Hickey et al.*, 1998; *Hickey and Brown*, 2002].

[5] The second method, described in section 2.1, uses certain approximations that allow the formulation of an analytical representation of airglow emission brightness fluctuations [*Swenson and Gardner*, 1998; *Swenson and Liu*, 1998; *Liu and Swenson*, 2003]. In the earlier studies the long-period gravity wave dispersion relation of *Hines* [1960] was used to describe the phase variation with height of a gravity wave undergoing adiabatic wave motion in an isothermal and windless atmosphere, while the more complete dispersion equation of *Hines* [1960] is utilized in *Liu and Swenson* [2003]. Wave amplitude is allowed to vary with height using a single predefined parameter β (which can be based on observation). A reduced set of chemical reactions pertinent to the particular airglow under study is used, and in the case of the OH airglow a set of parameters is used that is based on a fit to the observations of *McDade et al.* [1987]. Assuming that chemical lifetimes are much shorter than dynamical time constants, *Swenson and Gardner* [1998] (hereinafter referred to as SG98) derived a simple expression relating the perturbed VER to the mean VER and to perturbations in O, O_2 and temperature (T). The O_2 perturbation was defined explicitly in terms of the temperature perturbation by assuming quasi-hydrostatic gravity wave motions (for which pressure fluctuations are negligible). Fluctuations in O were defined using equations of *Gardner and Shelton* [1985] describing nonlinear fluctuations of a minor constituent. Integration over height of the VER provided the brightness fluctuation. SG98 relate this to the temperature perturbation at the altitude of maximum VER through a so-called "cancellation factor" (CF). Plots of the CF were presented for waves of various horizontal phase speeds for the OH airglow. One advantage of this approach is that it allows a simple look-up of CF for a given horizontal phase speed.

[6] It is the purpose of this paper to calculate a numerically based cancellation factor using the full-wave model [*Hickey et al.*, 1997, 1998, 2000a] and the chemical reaction scheme for the OH (8, 3) Meinel emission for gravity wave propagation in a nonisothermal, viscous, and windy atmosphere. Extensive comparisons will be performed between our numerically derived CF and the analytic CF of SG98 using various levels of approximation in the full-wave model, as described later. In this way we will be able to determine the atmospheric conditions for which the analytic CF of SG98 differs from the numerically derived CF. We will also be able to determine the influence of certain approximations on the derived CF's by performing specific sensitivity tests using our full-wave model. In this way, the limitations (if any) of the two models will be addressed, and our understanding of processes affecting gravity wave–driven airglow fluctuations will be improved. Ultimately the models must be able to describe the observations, and while the present work constitutes a model-to-model comparison and a model sensitivity study, we expect to be able to determine under what conditions the models should provide meaningful results.

[7] The layout of this paper is as follows. The model of SG98 is briefly described in section 2.1. The full-wave model, the chemical scheme, and the solution procedure of minor species fluctuations is described in section 2.2. The

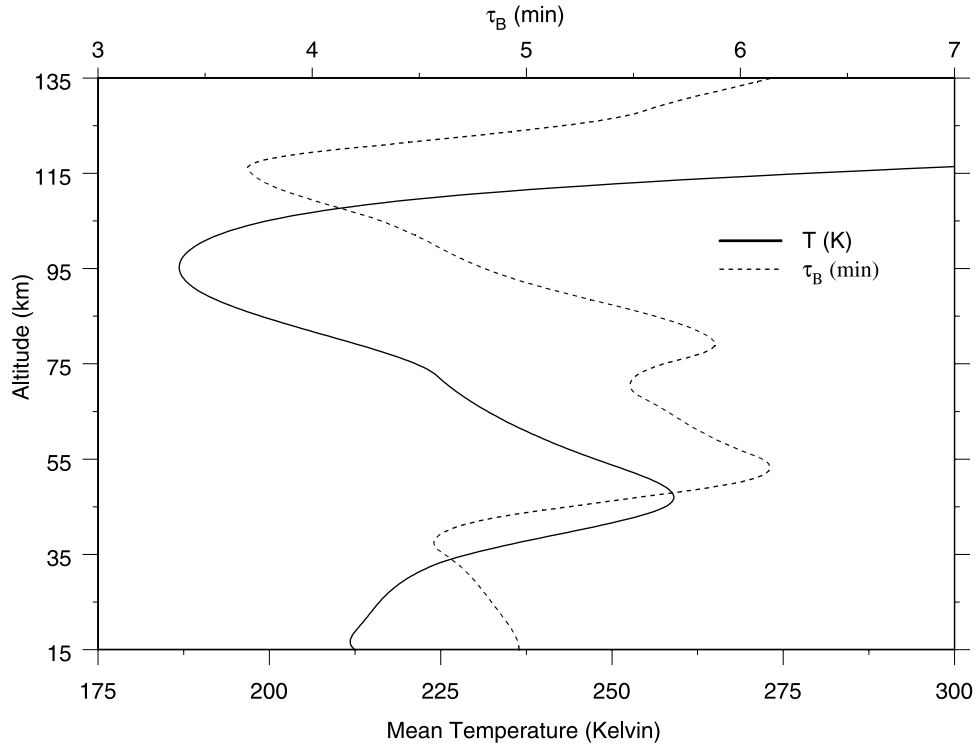

Figure 1. Mean atmospheric temperature for 15 December calculated from the MSIS-90 model (solid curve) and corresponding Brunt-Väisälä period (dashed curve).

results are presented in four subsections of section 3, covering a range of possible assumptions regarding the mean state. A discussion is presented in section 4, and conclusions are presented in section 5.

2. Methods for Determining Wave Amplitudes

2.1. Analytical Model of OH* Nightglow

[8] Using the solution procedure described by *Gardner and Shelton* [1985], SG98 derived expressions for the relative density fluctuations of the major gas and for a minor species. The altitude variation of these quantities was described by SG98 using the long-period dispersion equation of *Hines* [1960]

$$m^2 = \frac{(N^2 - \omega^2)}{\omega^2} k^2, \tag{1}$$

and later by *Liu and Swenson* [2003] (hereinafter referred to as the LS03 model) using the more complete dispersion equation of *Hines* [1960]

$$m^2 = \frac{(N^2 - \omega^2)}{\omega^2} k^2 - \frac{(\omega^2 - \omega_a^2)}{C^2}, \tag{2}$$

where k and m are the horizontal and vertical wavenumbers, respectively, and ω is the wave frequency. Also C is the sound speed, N is the Brunt-Väisälä frequency, and ω_a is the acoustic cutoff frequency, where $C^2 = \gamma gH$, $N^2 = (\gamma - 1)g^2/C^2$, $\omega_a = \gamma^2 g^2/4H^2$, and where γ is the usual ratio of specific heats, g is the gravitational acceleration, and H is the scale height.

[9] SG98 argued that because the lifetimes of OH* and ozone are short compared to typical gravity wave periods, the direct redistribution of OH* and O_3 by gravity waves is negligible. With this assumption, perturbations in the VER are solely determined by the perturbed O, O_2, and T profiles. SG98 derived the following equation describing fluctuations in the VER:

$$\begin{aligned}\Delta V(8,3) &= \frac{\partial V}{\partial [O]}\Delta[O] + \frac{\partial V}{\partial [O_2]}\Delta[O_2] + \frac{\partial V}{\partial T}\Delta T \\ &\approx \left(\frac{\Delta[O]}{[O]} + \frac{(2 + 7.7 \times 10^{-14}\text{cm}^3[O_2])\Delta[O_2]}{(1 + 7.7 \times 10^{-14}\text{cm}^3[O_2])\ [O_2]} \right. \\ &\quad \left. - 2.5\frac{\Delta T}{T}\right) V(8,3).\end{aligned} \tag{3}$$

Here Δ represents a perturbation about a mean, V is the VER, T is temperature, and the square brackets denote species concentrations. For quasi-hydrostatic (long period) gravity waves the pressure within a vertically displaced parcel continuously adjusts to the environmental pressure so that pressure fluctuations are negligible. SG98 made this assumption, giving

$$T/T_u = (\rho/\rho_u)^{-1}. \tag{4}$$

Here T_u and ρ_u are the unperturbed temperature and density, respectively, and T and ρ are the total (unperturbed plus perturbation) temperature and density, respectively. Note that although the quasi-hydrostatic assumption was subsequently relaxed in the LS03 model, the phase difference between density and temperature perturbations shown in

Table 1. Reactions and Kinetic Constants for OH (8, 3) Meinel Airglow

Reaction	Rate
$O + OH(\upsilon = 0) \rightarrow H + O_2$	$k_1 = 4.0 \times 10^{-11}$ cm^3/s
$H + O_2 + M \rightarrow HO_2 + M$	$k_2 = 2.1 \times 10^{-32}$ exp(290/T) cm^6/s
$O + HO_2 \rightarrow OH(\upsilon = 0) + O_2$	$k_3 = 4.0 \times 10^{-11}$ cm^3/s
$O + O + M \rightarrow O_2 + M$	$k_4 = 4.7 \times 10^{-33}(300/T)^2$ cm^6/s
$O + O_2 + M \rightarrow O_3 + M$	$k_5 = 1.0 \times 10^{-34}$ exp(510/T) cm^6/s
$H + O_3 \rightarrow OH * (\upsilon = 8) + O_2$	$k_6 = 0.27 \times 1.4 \times 10^{-10}$ exp(−470/T) cm^3/s
$OH * (\upsilon = 8) \rightarrow OH(\upsilon = 3) + h\upsilon$	$k_7 = 0.569$/s
$OH * (\upsilon = 8) + O \rightarrow H + O_2$	$k_8 = 2.5 \times 10^{-10}$ cm^3/s
$OH * (\upsilon = 8) + O_2 \rightarrow OH * (\upsilon - 1) + O_2$	$k_9 = 8.0 \times 10^{-12}$ cm^3/s
$OH * (\upsilon = 8) + N_2 \rightarrow OH * (\upsilon - 1) + N_2$	$k_{10} = 7.0 \times 10^{-13}$ cm^3/s

their Figure 1 does not asymptote to 180° at long wave periods, as it should when pressure fluctuations become negligible [e.g., *Walterscheid et al.*, 1987; *Hickey*, 1988b]. Therefore, when we use the LS03 model, we do so using a corrected WKB-derived relation between density and temperature perturbations.

[10] Integration over altitude of the VER fluctuations provides the airglow brightness fluctuation $\langle I' \rangle$

$$\langle I' \rangle = \int_0^\infty \Delta V(8,3) dz. \tag{5}$$

The CF is then calculated by SG98 using

$$CF = \left(\langle I' \rangle \Big/ \langle \bar{I} \rangle \right) \Big/ \left(T'/\bar{T} \right)_{z_{OH}}, \tag{6}$$

where the denominator represents the relative temperature fluctuation calculated at the altitude (z_{OH}) of the peak of the OH emission layer VER.

[11] In order to provide a meaningful model-to-model comparison, our implementation of the SG98 model diverges slightly from that of SG98 because whereas they used a Chapman function to fit the MSIS-90 model O densities, we do not. We do not use equation (25) of SG98 (nor do we use the equations based on using their equation (25)). Instead, the relative perturbations in the atomic oxygen profile are computed using their equations (2) and (6) with the undisturbed O profile given by the MSIS−90 model [*Hedin*, 1991]. This is done to standardize as many of the inputs as possible used in the full-wave model and in the (modified) SG98 model.

[12] Another difference arises because the chemical rate constants used by SG98 are not exactly the same as those used by *Hickey* [2001a] in a full-wave study of gravity waves in the OH nightglow, and so we have repeated the SG98 derivation of their equations (15), (17), and (19) with the same rate constant used in the full-wave model for the three-body recombination $O + O_2 + M \rightarrow O_3 + M$. This rate constant ($k_5 = 1.0 \times 10^{-34}$exp(510/$T$) cm^6/s) is given in Table 1. We obtain

$$\begin{aligned} \Delta V(8,3) &= \frac{\partial V}{\partial [O]} \Delta [O] + \frac{\partial V}{\partial [O_2]} \Delta [O_2] + \frac{\partial V}{\partial T} \Delta T \\ &\approx \left(\frac{\Delta [O]}{[O]} + \frac{(2 + 7.7 \times 10^{-14} \text{cm}^3 [O_2]) \Delta [O_2]}{(1 + 7.7 \times 10^{-14} \text{cm}^3 [O_2])\ [O_2]} \right. \\ &\quad \left. - 510 \frac{\Delta T}{T^2} \right) V(8,3). \end{aligned} \tag{7}$$

We replace equation (3) by equation (7) when we use the SG98 model to calculate the analytical CF.

2.2. Full-Wave Model With Chemical Scheme

[13] The full-wave model provides solutions to the coupled continuity, momentum, energy, and ideal gas equations. The model includes dissipation due to eddy processes in the lower atmosphere and molecular processes (viscosity, thermal conduction, and ion drag) in the upper atmosphere. Height variations of the horizontal winds and mean temperature, as well as the Coriolis force are all included [*Hickey et al.*, 1997, 1998, 2000a]. The governing equations of wave propagation are

$$\frac{D\rho}{Dt} + \rho \underline{\nabla} \cdot \underline{v} = 0, \tag{8}$$

$$\begin{aligned} \rho \frac{D\underline{v}}{Dt} &+ \underline{\nabla} p - \rho \underline{g} + 2\rho \underline{\Omega} \times \underline{v} + \underline{\nabla} \cdot \underline{\underline{\sigma}}_m + \underline{\nabla} \cdot (\rho \eta_e \underline{\nabla} \underline{v}) \\ &+ \rho \nu_{ni} (\underline{v} - \underline{v}_i) + \rho K_R \underline{v} = 0, \end{aligned} \tag{9}$$

$$\begin{aligned} \rho \frac{D(c_V T)}{Dt} &+ p \underline{\nabla} \cdot \underline{v} + \underline{\underline{\sigma}}_m : \underline{\nabla} \underline{v} - \underline{\nabla} \cdot (\lambda_m \underline{\nabla} T) - c_V \frac{\overline{T}}{\overline{\theta}} \underline{\nabla} \cdot [\rho \kappa_e \underline{\nabla} \theta] \\ &+ \rho \nu_{ni} (\underline{v} - \underline{v}_i)^2 + c_V \rho K_N T = 0, \end{aligned} \tag{10}$$

$$p = \frac{\rho R T}{M}. \tag{11}$$

These equations are linearized and used to describe fully compressible, two-dimensional waves. $\underline{v}$ is the velocity with x (positive southward), y (positive eastward), z (positive upward) components u, v and w, respectively; ρ is the neutral mass density; p is atmospheric pressure; g is the gravitational acceleration; Ω is the Earth's angular velocity; $\underline{\underline{\sigma}}_m$ is the molecular viscous stress tensor; η_e is the eddy momentum diffusivity; ν_{ni} is the neutral-ion collision frequency; $\underline{v}_i$ is the ion velocity; c_P and c_V are the specific heats at constant pressure and volume, respectively; T is temperature; λ_m is the molecular thermal conductivity; κ_e is the eddy thermal diffusivity; M is the mean molecular weight; and K_R and K_N are the Rayleigh friction and Newtonian cooling coefficients, respectively [*Hickey et al.*, 2000a].

[14] The operator $D/Dt = \partial/\partial t + \underline{v} \cdot \underline{\nabla}$ is the substantial derivative, where $\underline{v}(z)$ is the total wind (mean plus perturbation). θ is the potential temperature (θ =

$T(\overline{p}_{00}/p)^{\kappa}$), where $\overline{p}_{00}$ = 1000 mbar, $\kappa = R/c_P$, and R is the gas constant.

[15] The chemical reaction scheme for OH (8, 3) Meinel emission used in the full-wave model describes the production and loss of OH* as described in Table 1. The excited hydroxyl (OH*) is produced by the reaction of atomic hydrogen with ozone, and lost through several vibrational band emissions and through quenching by O, O_2, and N_2.

[16] The number density n of the minor species is determined using the linearized continuity equation [*Walterscheid et al.*, 1987]

$$\frac{\partial n'}{\partial t} = P' - L' - \frac{d\,\overline{n}}{dz} w' - \overline{n}\underline{\nabla} \cdot \underline{v}', \tag{12}$$

where it has been assumed that all species have the same temperature T and velocity $\underline{v}$ as the major gas. The terms P and L are rates of volumetric production and loss of minor constituents by chemical reactions. Primes denote perturbed quantities, overbars denote unperturbed quantities, z is altitude, and w is the vertical velocity. The concentration of O changes slowly during the night compared with the fluctuation time scale of interest (gravity wave periods of minutes to hours), so that we consider the basic state as steady [*Walterscheid et al.*, 1987].

[17] Assuming that the perturbations are due to plane waves propagating in the x - z plane (x is the horizontal coordinate) we write

$$(n', T', \underline{v}', \ldots) = \left[\hat{n}(z), \hat{T}(z), \underline{\hat{v}}(z), \ldots\right] \exp i(\omega t - kx), \tag{13}$$

where a circumflex denotes the z - dependent part of the fluctuation. Substitution of (13) into (12) then yields

$$i\omega\hat{n} = \hat{P} - \hat{L} - \frac{d\,\overline{n}}{dz}\hat{w} - \overline{n}\underline{\nabla} \cdot \underline{\hat{v}}. \tag{14}$$

[18] The solution of (14) has been described before by *Walterscheid et al.* [1987], *Hickey* [1988a, 1988b], and in the case of the full-wave model by *Hickey et al.* [1997] and *Hickey* [2001a]. All forcing terms in (14) (those explicitly involving the gravity wave perturbations $\hat{T}$, $\underline{\hat{v}}$, $\hat{\rho}$ and $\underline{\nabla} \cdot \underline{\hat{v}}$) are moved to the right side of the equation while all unknown minor species density fluctuation terms are moved to the left side of the equation. The system of minor species continuity equations (14) representing fluctuations in OH*, OH, O_3, H, O, and HO_2 are thus written as

$$\begin{bmatrix} 6\times 6 \\ matrix \end{bmatrix} \begin{bmatrix} \hat{n}(OH^*) \\ \hat{n}(OH) \\ \hat{n}(O_3) \\ \hat{n}(H) \\ \hat{n}(O) \\ \hat{n}(HO_2) \end{bmatrix} = \begin{bmatrix} 6\times 1 \\ matrix \end{bmatrix} \left(\frac{\hat{T}}{\overline{T}}\right). \tag{15}$$

[19] The OH chemistry used in the full-wave model is provided in Table 1. The matrices appearing in (15) are derived from Table 1 by calculating the volumetric production (P) and loss rates (L) of minor constituents. A straightforward inversion of (15) yields the $\hat{n}$ solution vector for the perturbation number densities of the minor constituents. This approach has been used in the full-wave model by *Hickey et al.* [1997, 1998] to simulate gravity wave effects in the OI 5577 airglow, by *Hickey and Walterscheid* [1999] to simulate gravity wave effects in the O_2 atmospheric airglow, and by *Hickey* [2001a], *Hecht et al.* [2002] and *Huang et al.* [2002] to simulate gravity wave effects in the OH airglow. Minor species are provided from the model of *Garcia and Solomon* [1985] for a latitude of 39°N and for December, as supplied by R. Garcia (private communication, 1990). However, the O and H number densities and rate constants were used to provide the steady-state minor species distributions for O_3, HO_2, OH and OH*. To facilitate comparison with the SG98 model described in section 2.1, the full-wave model chemistry uses O number densities obtained from the MSIS-90 model [*Hedin*, 1991].

3. Results and Analyses

[20] In this section we compare the CFs calculated from the full-wave model with those calculated from the analytic model of *Swenson and Gardner* [1998] (SG98). We consider horizontal wavelengths (λ_h) of 100 km and 500 km. For each value of λ_h we consider 100 different waves with intrinsic phase speeds ranging from 30 m s^{-1} to 180 m s^{-1}. We also consider varying those mean state parameters that are expected to influence the derived CF's. We are particular interested in determining the sensitivity of the CF to various physical processes nominally included in the full-wave model. In the following sections we examine the sensitivity of the CF's derived from the full-wave model to the inclusion of a nonisothermal atmosphere, eddy diffusion, and mean background winds. Effects associated with the Coriolis force that are nominally described in the full-wave model are not included here because for the range of wave parameters considered we expect it to be less important than these other processes.

[21] In the present study we could have considered examining the sensitivity of values of CF derived from the two models to other influences, such as season, time of day, and latitude. We do not do so due to space limitations, and furthermore it is our belief that these factors would influence the CF's derived from the two models in similar ways and would therefore not emphasize model differences. When we compare the CF calculated for a nonisothermal atmosphere to the CF calculated for an isothermal atmosphere, we must recognize that both the dynamics and chemistry may be influenced by differences in the mean temperature structure. Our primary goal is to understand the impact of different assumptions used in the dynamical models. In order to minimize the impact of using two different assumed mean temperature profiles in the chemistry, we set the temperature for the isothermal atmosphere equal to the temperature in the vicinity of peak VER for the OH airglow (z_{OH}). In this way, chemical rate constants and the VER profile itself will be similar for the isothermal and nonisothermal cases (which we have verified).

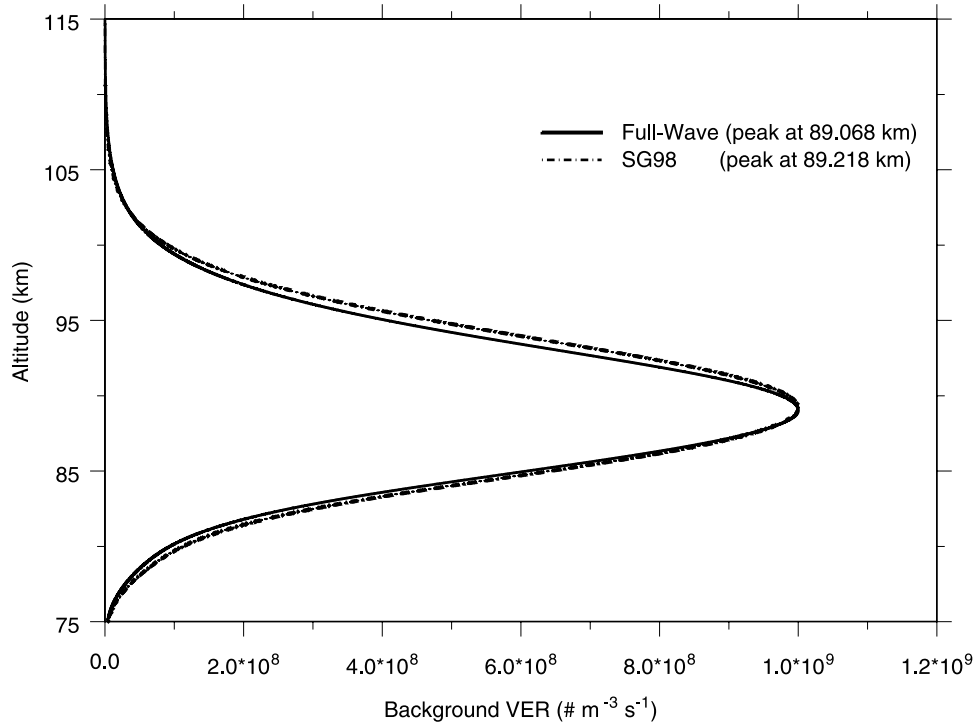

Figure 2. The background volume emission rate (VER) profile derived from the full-wave (solid curve) and SG98 (dashed-dotted curve) models.

[22] The mean temperature (solid curve) for 15 December derived from the MSIS-90 model [*Hedin*, 1991] and the corresponding nonisothermal Brunt-Väisälä period (dashed curve) are plotted as function of altitude in Figure 1. These results (and those to follow) are based on mid-latitude (39°N) nighttime conditions. The mesopause is situated at about 96 km altitude with a temperature of about 186 K, and the large temperature gradient in the lower thermosphere is clearly evident. When an isothermal atmosphere is considered the temperature is fixed at a value of ~194.7 K (the value at the altitude of the maximum VER for the OH airglow). Note that this value is close to the value of 200 K used by *Swenson and Gardner* [1998]. The value of the Brunt-Väisälä period (dashed curve) in the vicinity of the OH airglow layer (~87 km) means that the shortest allowed periods for internal gravity waves is ~5 min. Upward propagating gravity waves with periods less than about 10 to 12 min will be reflected back downward from thermospheric altitudes, which may lead to ducting [*Walterscheid et al.*, 1999; *Hecht et al.*, 2001; *Hickey*, 2001b] and wave interference effects in the airglow, effects that are accounted for in the full-wave model.

[23] The unperturbed VER for the OH airglow for each of the two models is plotted as function of height in Figure 2. The two different chemical schemes representing the OH airglow are different, as described earlier, and lead to different maximum values of the VER. The actual maximum value of the VER is not as important as the profile shape because the CF is the ratio between the perturbed and unperturbed VER, both of which will differ between the two models. Hence we have normalized the two profiles such that they both have the same maximum VER of 10^9 m^{-3} s^{-1}. The altitude of maximum VER occurs at z_{OH} ~ 89.1 km for the full-wave model (solid curve) and at ~89.2 km for the SG98 model (dashed-dotted curve). The thicknesses of the two VER profiles are very similar to each other, with a full-width at half-maximum of ~9.9 km for the full-wave model and ~10.7 km for the SG98 model.

[24] The SG98 model includes the generalized nonlinear gravity wave solutions of *Gardner and Shelton* [1985], whereas the full-wave model is linear. We compare these two models using small amplitudes to ensure that the gravity waves are linear in the SG98 model. In order to determine the range of wave amplitudes for which the CF behaves linearly in the SG98 model we first compare the CF's calculated using the SG98 analytic model alone for relative temperature fluctuation amplitudes of 0.1%, 1%, 5% and 10% at the altitude of the OH* emission layer peak (z_{OH}). The results (not shown) demonstrate that the CF behaves approximately linearly for wave amplitudes at z_{OH} of less than or equal to 1%, and strongly nonlinearly for wave amplitudes at z_{OH} greater than 1%. We therefore compare the CF's derived from the two models using a value of 0.1% for the relative temperature fluctuation amplitude at z_{OH}.

[25] In order to compare the influences of chemistry and dynamics on the OH nightglow, *Walterscheid et al.* [1987] inferred chemical time constants in an operational sense by determining the time scales at which significant differences existed between model results obtained based on including chemistry and dynamics together with those based on including dynamics alone. Commonly, chemical time constants are calculated from the chemical loss rate of each species, but nonlinear chemistry causes the system to be highly coupled so that this method can give erroneous results [*Prather*, 1994; *Xu and Smith*, 2003]. The chemical time

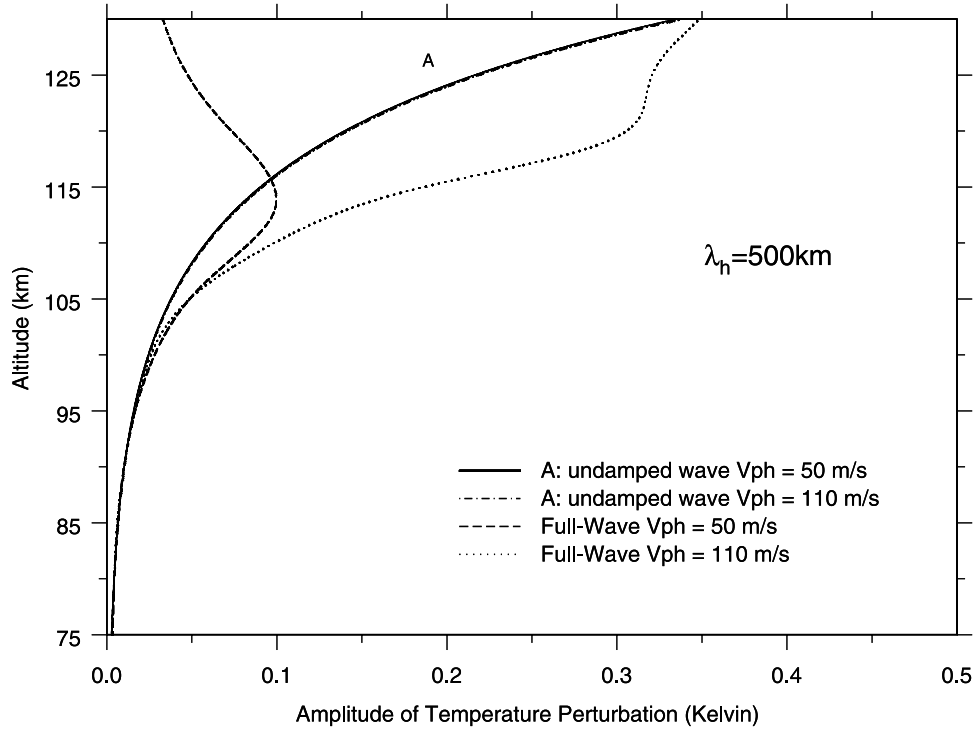

Figure 3. Temperature perturbation amplitude for a λ_h = 500 km gravity wave calculated from the SG98 model (nonisothermal and nonadiabatic atmosphere) for V_{ph} = 50 m/s (A, solid curve) and V_{ph} = 110 m/s (A, dashed-dotted curve). The temperature perturbation amplitude calculated from the full-wave model (nonisothermal and nonadiabatic atmosphere) is also shown for V_{ph} = 50 m/s (dashed curve) and for V_{ph} = 110 m/s (dotted curve).

constant for O_3 is of the order of 10 min, so that dynamical and chemical time scales are comparable. The chemical time constants for H and O are longer than 10 hours, which is longer than typical gravity wave periods of interest [*Walterscheid et al.*, 1987]. Here we also use the approach of *Walterscheid et al.* [1987] in order to evaluate the dominance of dynamics or chemistry in the calculated CF in the full-wave model (note that we do not perform such sensitivity tests using the SG98 model). In the case of dynamics alone, we set all rate constants equal to zero in the full-wave model in the evaluation of minor species perturbations (that is, in equation (15)). In the case of chemistry alone in the full-wave model the major gas fluctuations $\underline{\hat{v}}$, $\hat{\rho}$ and $\underline{\nabla}\cdot\underline{\hat{v}}$ are set to zero on the right side of (15).

3.1. Wave Amplitude Profiles

[26] We compare the propagation of gravity waves in a nonisothermal atmosphere (full-wave model) to that for an isothermal atmosphere (SG98 model) by choosing two gravity waves having intrinsic phase speeds of 50 m/s and 110 m/s, and each having a horizontal wavelength of 500 km. The amplitude of the temperature perturbation for each of these waves (which are all equal at height z_{OH}) is plotted as the function of altitude in Figure 3. The results derived from the full-wave model show that the faster gravity wave (larger vertical wavelength, dotted curve) is less dissipated than the slower gravity wave (smaller vertical wavelength, dashed curve), as expected [e.g., *Pitteway and Hines*, 1963; *Richmond*, 1978]. The SG98 model primarily considers undamped gravity waves but it can include damping by setting a parameter β to be nonzero (as discussed later). The two temperature perturbation amplitude profiles derived using a value of $\beta = 0$ in the SG98 model and labeled "undamped wave" in Figure 3 exhibit identical variations with altitude. In addition, in the SG98 model the gravity waves grow exponentially with height with a constant scale-height. In the full-wave model the scale-height (not shown) and mean temperature vary continuously with height and so consequently, below ~110 km altitude, the wave amplitude of the faster (undamped) gravity wave grows at a faster rate than it does in the isothermal SG98 model. This means that fluctuations in temperature (and also in the VER) will be essentially larger above z_{OH} in the nonisothermal full-wave model than in the SG98 model. This will contribute to differences between CF's derived for an isothermal atmosphere and those derived for a nonisothermal atmosphere.

[27] In addition to the amplitude profiles shown in Figure 3 we also considered the case of a constant amplitude over altitude in the LS03 model (not shown) by setting their β equal to unity. This value of β mimics wave saturation associated with breaking gravity waves [*Fritts*, 1984]. Results obtained using values of $\beta = 0$ and $\beta = 1$ are considered in our comparisons.

3.2. Isothermal Atmosphere

[28] Here the atmosphere is assumed to be isothermal with a constant mean temperature of ~194.7 K as previously discussed. Full-wave model results are presented for calculations based on complete dissipation (nonadiabatic) and reduced dissipation (quasi-adiabatic). For quasi-

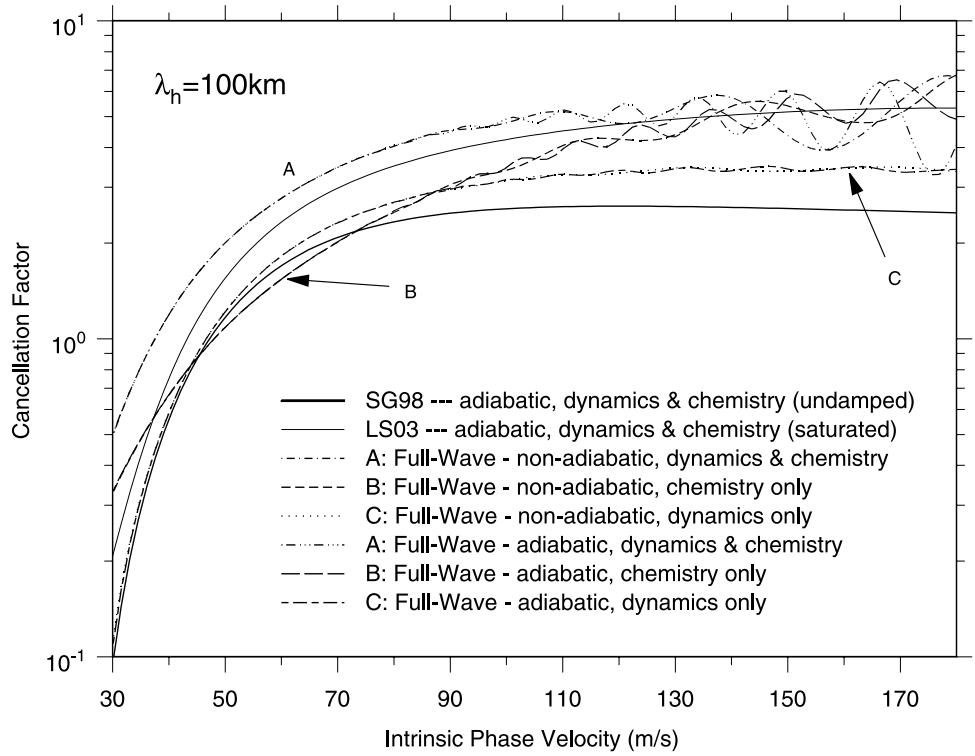

Figure 4. The CF plotted as a function of gravity wave intrinsic phase speed for λ_h = 100 km and calculated for an isothermal atmosphere. Results are shown for the SG98 model (thick solid curve) and for the LS03 model (thin solid curve). Nonadiabatic full-wave model results are shown based on dynamics and chemistry together (A, dashed-dotted curve), chemistry alone (B, short-dashed curve), and dynamics alone (C, dotted curve). Quasi-adiabatic full-wave model results are shown based on dynamics and chemistry together (A, dashed-triple-dotted curve), chemistry alone (B, long-dashed curve), and dynamics alone (C, long-dashed, short-dashed curve).

adiabatic simulations the molecular diffusion coefficients in the full-wave model are all significantly reduced to a fraction of their nominal values. In addition, the eddy diffusivity is taken to be a constant equal to a small "background" component ($\sim$0.1 m^2 s^{-1}).

[29] The CF's derived from the SG98 and full-wave models for λ_h = 100 km are shown in Figure 4. The wave intrinsic phase speeds range from 30 m s^{-1} to 180 m s^{-1} corresponding to wave periods ranging from $\sim$55 min to $\sim$9 min, respectively. For all results shown the vertical wavelength decreases as the phase speed decreases, causing the CF to decrease due to increased destructive interference over altitude between the positive and negative fluctuations in VER [*Schubert et al.*, 1991; *Hines and Tarasick*, 1994; *Taylor et al.*, 1995; *Swenson and Gardner*, 1998; *Walterscheid et al.*, 1999].

[30] The full-wave results presented in Figure 4 show that the CF's derived from the full-wave model are insensitive to the dissipation in the model for gravity waves with phase speeds less than about 90 m s^{-1}. For the faster gravity waves shown with phase speeds greater than about 90 m s^{-1} the calculated CF's display undulations that arise due to the effects of reflection from the middle thermosphere ($\sim$250 km altitude) associated mainly with evanescence (with some contribution from the effects of strong gradients in temperature and molecular diffusion). This reflection that affects faster gravity waves is discussed in more detail in the discussion section. The differences arising between the adiabatic and nonadiabatic cases are due to the larger amplitude of the downward propagating (reflected) gravity wave in the airglow region in the adiabatic case associated with less dissipation.

[31] In order to assess the relative importance of dynamical and chemical effects in the full-wave model, in Figure 4 we also compare the CF's obtained with all processes included together (curves labeled "A") with those obtained considering either chemistry ("B") or dynamics ("C") alone. For the fast high-frequency gravity waves (periods $\sim$10 min to 15 min) the CF's calculated including all processes together (dashed-triple-dotted curve, labeled "A") are similar to those derived including chemistry alone (long-dashed curve, labeled "B"). The CF's derived from the full-wave model including all processes together (dashed-triple-dotted curve, labeled "A") approach the CF's derived including chemistry alone (long-dashed curve, labeled "B") for high frequency gravity waves. Overall comparison between the full-wave model results obtained including all processes (curves "A") and neglecting either chemistry or dynamics (curves "B" and "C") shows that all processes need to be included in the calculation of the CF over a broad range of phase speeds and wave periods.

[32] The SG98 model CF and LS03 model CF are also compared to the full-wave model CF's in Figure 4. The SG98 model CF (thick solid curve) is always smaller than

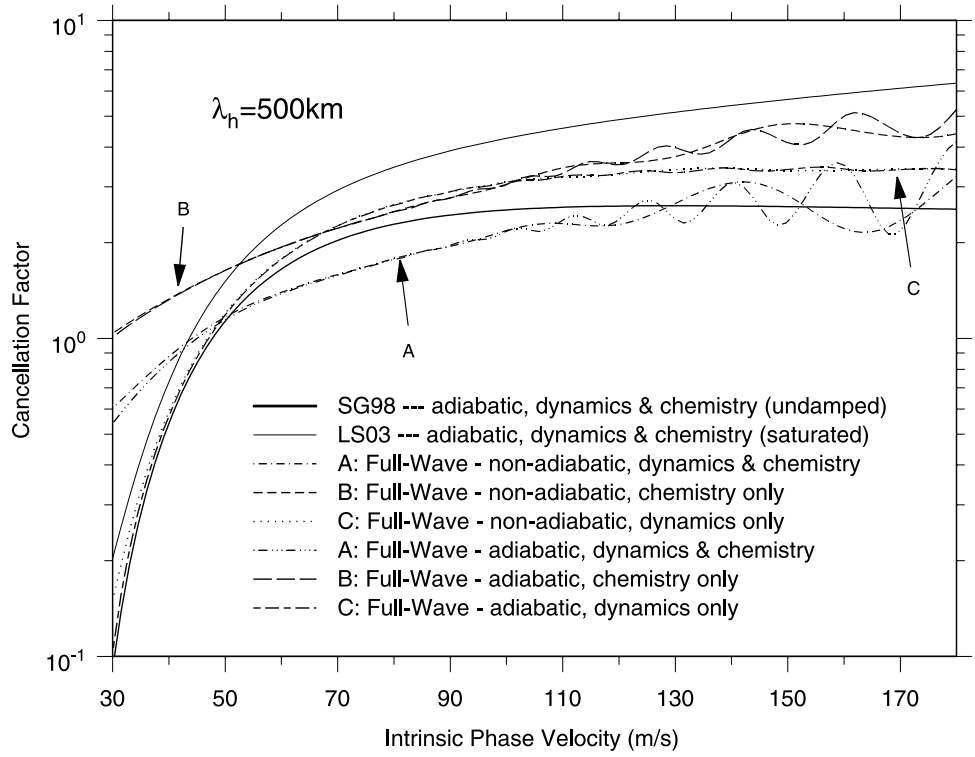

Figure 5. Similar to Figure 4, except for λ_h = 500 km.

the full-wave model CF calculated including all processes (curves "A"). For the slower gravity waves considered with phase speeds between 30 m s^{-1} and ~50 m s^{-1} the SG98 model CF's and full-wave model with dynamics only CF's (curves "C") agree remarkably well with each other. For the faster gravity waves the LS03 model CF's based on saturation (β = 1) (thin solid curve) are comparable to the full-wave model CF's that include chemistry (curves "A" and "B"). For the slower gravity waves the LS03 model CF's equal the approximate average of the two full-wave model CF's that include chemistry (curves "A" and "B"). It is also interesting to note that the SG98 model CF's (thick solid curve) and the full-wave model including dynamics only CF's (dotted curve and long-dashed, short-dashed curve) are very similar for gravity waves with phase speeds of less than about 60 m s^{-1}.

[33] The CF's derived from the SG98, LS03 and full-wave models are shown for λ_h = 500 km in Figure 5. The wave intrinsic phase speeds range from 30 m s^{-1} to 180 m s^{-1} with corresponding wave periods ranging from ~4 hours 37 min to ~46 min, respectively. As noted for the λ_h = 100 km results, the full-wave model CF's exhibit undulations as a function of phase speed for phase speeds greater than about 100 m s^{-1} as a consequence of the effects of wave reflection, as explained more completely in the discussion. The CF's derived from the full-wave model including all processes together (dashed-triple-dotted curve, "A") and including chemical process alone (long-dashed curve, "B") differ by a factor of ~2 from each other for slow gravity waves having periods of several hours. The CF's based on chemistry alone exceeds that due to dynamics and chemistry at these periods. At these long periods the smallest CF's arise in the case of dynamics alone. For the longest period gravity waves and for dynamics and chemistry included together (dashed-triple-dotted curve, "A") the CF's derived from the full-wave model are greater by a factor of ~6 than those derived from the SG98 model (thick solid curve), suggesting that for a given wave amplitude the full-wave model predicts that a gravity wave may be more easily observed in the airglow than the SG98 model would suggest. It is interesting to note that the SG98 model CF's (thick solid curve) and the full-wave model including dynamics only CF's (dotted curve and long-dashed, short-dashed curve) are very similar for gravity waves with phase speeds of less than about 70 m s^{-1}.

[34] For the λ_h = 500 km gravity wave the full-wave model CF's are more influenced by dissipation in the low frequency region compared to the results discussed for the λ_h = 100 km gravity wave in Figure 4. However, the effects of dissipation do not have a dominant influence on derived values of CF at any wave period for the λ_h = 500 km gravity wave. Therefore, for the remainder of the results section, only quasi-adiabatic simulations (neglecting dissipation) will be considered.

3.3. Nonisothermal Atmosphere

[35] In this case the nonisothermal mean temperature profile of 15 December calculated from the MSIS-90 model is employed (Figure 1), and the diffusion coefficients previously used to represent quasi-adiabatic motions are used, as described in section 3.2. Results are presented only for the full-wave model because we are specifically interested in exploring the effects of a nonisothermal mean state atmosphere on gravity waves in the airglow, which the SG98 and LS03 models do not include.

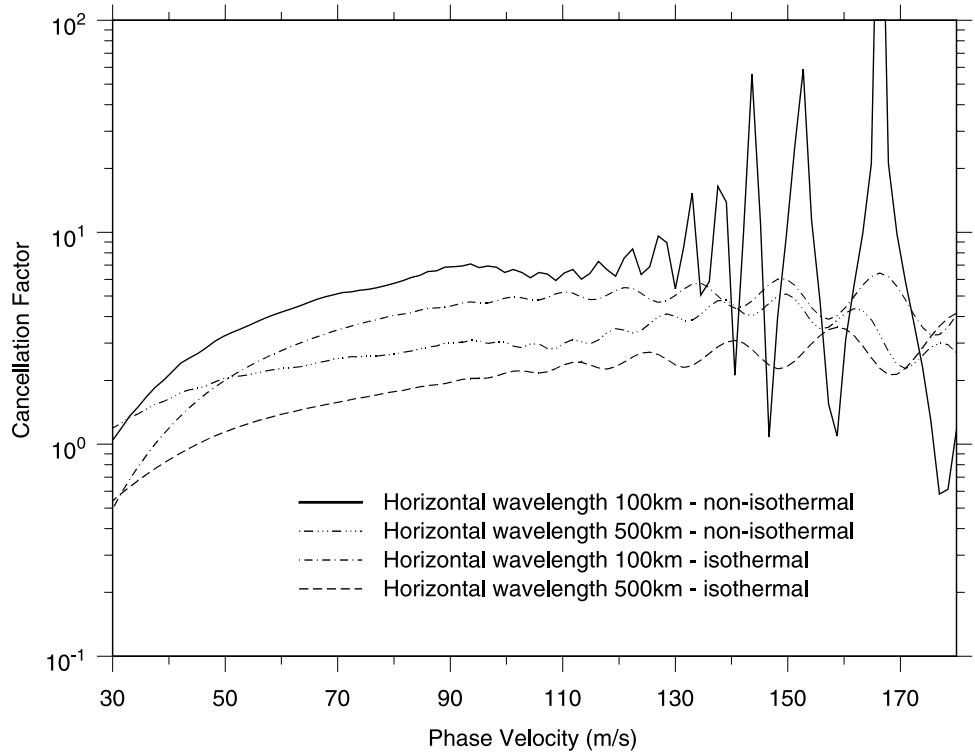

Figure 6. The CF calculated using the full-wave model for quasi-adiabatic conditions based on including dynamics and chemistry together and plotted as a function of gravity wave intrinsic phase speed. Results are shown for a nonisothermal atmosphere and for λ_h = 100 km (thick solid curve) and λ_h = 500 km (dashed, triple-dotted curve), and for an isothermal atmosphere and for λ_h = 100 km (dashed-dotted curve) and for λ_h = 500 km (long-dashed curve).

[36] The CF's derived from the full-wave model including both dynamics and chemistry are shown in Figure 6 for λ_h = 100 km and for λ_h = 500 km and for gravity wave propagation in both an isothermal and nonisothermal atmosphere. For a given value of horizontal wavelength and for phase speeds smaller than about 130 m s^{-1} the CF's calculated for a nonisothermal atmosphere are greater than those calculated for an isothermal atmosphere. This is expected based on the results shown previously in Figure 3, where gravity wave amplitudes are larger in a nonisothermal atmosphere at altitudes above the peak of the OH emission layer. For waves with phase speeds greater than about 100 m s^{-1} the CF's exhibit undulations whose amplitude increases with increasing phase speed. This is particularly so for the λ_h = 100 km gravity waves propagating in a nonisothermal atmosphere, where extremely large undulations in the CF are seen. These waves experience reflection in the middle to lower thermosphere region where they become evanescent due to the local Brunt-Väisälä period increasing to a value greater than the wave periods. In the case of gravity wave propagation in an isothermal atmosphere the strong height variation of wave dissipation leads to a breakdown in the WKB approximation for fast gravity waves having large vertical wavelengths and strong reflection occurs [*Lindzen*, 1968; *Yanowitch*, 1967, 1969; *Chapman and Lindzen*, 1970]. Within the airglow region the faster upward and downward propagating gravity waves interfere leading to undulations in the calculated CF's. These effects and their relevance to observations are discussed in more detail in the section 4.

3.4. Effects of Mean Winds

[37] Mean winds cause a Doppler shifting of gravity wave frequencies with important consequences for propagation. If the horizontal wind speed equals the horizontal phase trace speed at any particular level (the so-called "critical level") the Doppler shifted frequency (intrinsic frequency) is zero and the wave is either absorbed in the mean flow or partially reflected depending on the local Richardson number [*Booker and Bretherton*, 1967; *Hines and Reddy*, 1967; *Jones*, 1968; *Breeding*, 1971; *Bowman et al.*, 1980]. Alternatively, a wave propagating in a direction opposite to the mean wind is Doppler shifted to higher frequencies towards the local Brunt-Vaisala frequency, and will be reflected for a large enough wind. The diurnal winds act as a time-dependent filter of gravity waves propagating upward into the thermosphere producing an observed time-dependent direction of preferred propagation [*Cowling et al.*, 1971; *Morton and Essex*, 1978; *Waldock and Jones*, 1984]. A similar preferred direction of gravity wave propagation has been observed in the mesopause region [*Taylor et al.*, 1993]. The most striking example of the effects of mean winds on gravity wave propagation directions is associated with the seasonal variation of stratospheric winds, which preferentially block eastward propagating gravity waves during winter and westward propagating gravity waves during summer. The subsequent momentum deposition in the mesosphere due

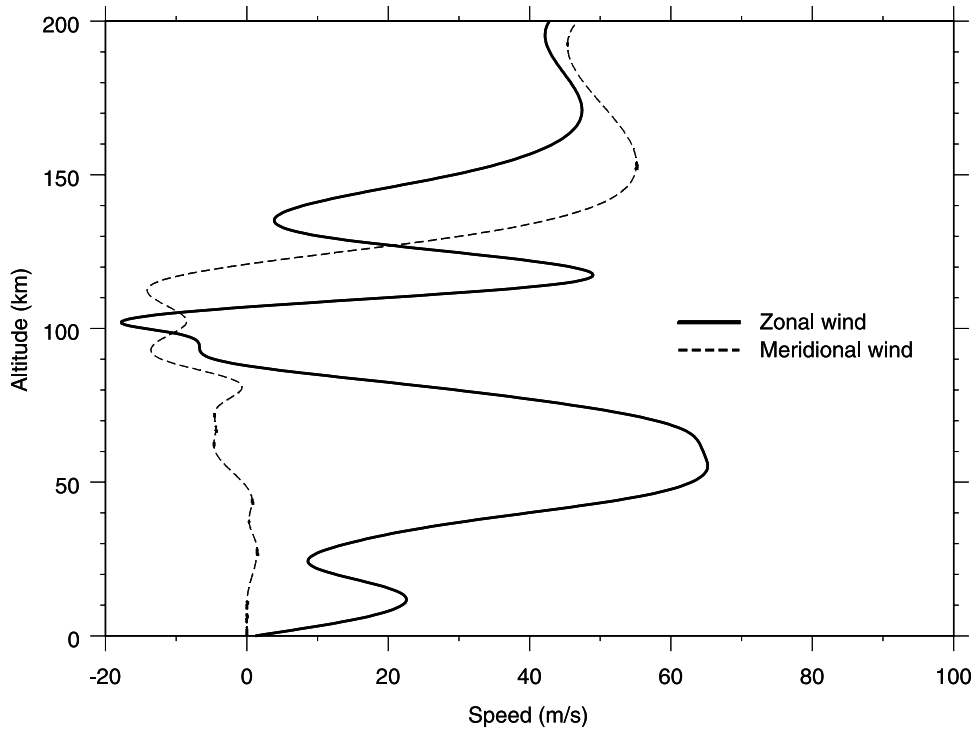

Figure 7. The meridional (positive southward, dashed curve) and zonal (positive eastward, solid curve) wind profiles for winter (15 December).

to breaking gravity waves drives a diabatic circulation that is responsible for the cold summer/warm winter mesopause temperatures [*Lindzen*, 1981; *Holton*, 1982].

[38] In this section the effect of background winds on derived cancellation factors is determined using the full-wave model including all processes together (dynamics, chemistry, and a nonisothermal mean state) by including empirical mean winds prescribed using the Horizontal Wind Model (HWM) [*Hedin et al.*, 1996]. Cancellation factors are not presented for the SG98 and LS03 models because they do not include wind effects. Although mean winds vary with position (altitude, latitude, and longitude), season and local time (and also with the level of solar and geomagnetic activity at thermospheric altitudes), we consider only two wind profiles, one representing summer and the other representing winter. Detailed results are presented for the winter winds, while the summer wind results are only briefly discussed. Consideration of a larger number of different wind profiles in our simulations is beyond the scope of this paper.

[39] *Hickey and Brown* [2002] demonstrated that realistic mean winds (as provided, for example, by lidar measurements) can significantly influence the airglow response to certain gravity waves propagating through airglow emission layers. In particular, it was discovered that the existence of critical levels within the airglow layers, where the gravity wave intrinsic phase speed is zero, had a profound influence on the airglow response to the waves. Unfortunately, the HWM mean winds do not lead to critical levels in the vicinity of the OH airglow region for any of the gravity waves we consider, and so some of the more interesting effects associated with realistic winds cannot be assessed here.

[40] Simulations are performed for the northern hemisphere winter (15 December) using the mean state temperature (Figure 1) and nominal eddy diffusion coefficients discussed earlier. The altitude variations of the mean meridional and zonal winds are shown in Figure 7. The zonal wind (solid curve) is larger than the meridional wind (dashed curve) throughout the middle atmosphere including much of the OH airglow region. The strong wintertime eastward (westerly) winds throughout the stratosphere and the lower mesosphere leads to critical level filtering (blocking) of eastward propagating gravity waves with phase speeds less than about 65 m s^{-1} so that these waves will not reach the airglow region in the upper mesosphere. Consequently, we do not present the calculated CF's for waves with eastward phase speeds of less than about 65 m s^{-1}. For altitudes between 80 km and 100 km (the approximate bottom side and top side, respectively, of the OH VER layer, as seen in Figure 2) the maximum meridional and zonal wind speeds are $\sim$14 m s^{-1} and $\sim$30 m s^{-1}, respectively. Thus, within the airglow region, wind speeds are quite modest. At slightly higher altitudes ($\sim$150 km) both the meridional and zonal wind speeds are about 50 m s^{-1}, which can influence the derived CF's for some of the shorter period waves, as described in the discussion section.

[41] The cancellation factors are shown as a function of extrinsic phase speed for λ_h = 100 km in Figure 8. With the inclusion of mean winds wave propagation in the eastward (solid curve), westward (dashed-triple-dotted curve), northward (dashed-dotted curve) and southward (long-dashed curve) directions was considered. Without loss of generality, wave propagation was considered in the eastward direction in the windless case (short-dashed curve). For eastward propagation with winds (solid curve) the CF increases

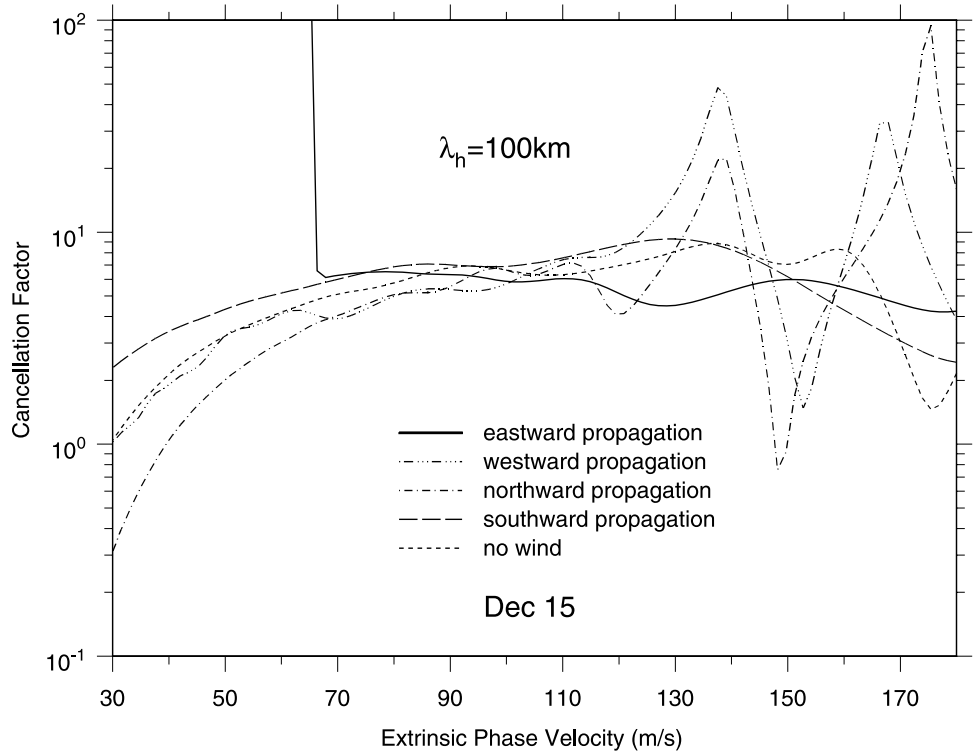

Figure 8. The CF calculated using the full-wave model for nonadiabatic conditions based on including dynamics and chemistry together and plotted as a function of gravity wave extrinsic phase speed. Results are based on wintertime (15 December) excluding background winds (short-dashed curve), and also including background winds with eastward propagation (solid curve), westward propagation (dashed, triple-dotted curve), northward propagation (dashed-dotted curve), and southward propagation (long-dashed curve).

dramatically for the slower phase speed waves shown ($\leq$65 m s^{-1}), which results from critical level encounters in the middle part of the mesosphere. As previously noted, these waves would not reach airglow altitudes and so the associated CF's (and their apparently erratic behavior) are moot and therefore not shown.

[42] Comparison of the various curves in Figure 8 shows that the CF's calculated for the fastest gravity waves with phase speeds exceeding about 120 m/s appear to be strongly influenced by the mean winds. As will soon be discussed, gravity wave events derived from airglow observations rarely (if ever) reveal gravity waves having very large propagation speeds ($\geq$100 m/s), and so results for these fast waves are unlikely to be relevant to observations. The CF's calculated without winds (short-dashed curve in Figure 8) increase monotonically from a value near unity for a 30 m/s gravity wave up to a value of about 7 at 90 m/s. For phase speeds greater than 90 m/s the calculated CF's display undulations that increase in amplitude with increasing phase speed. Qualitatively similar behavior is seen in the variation of CF with phase speed when winds are included for both northward propagation (dashed-dotted curve) and westward propagation (dashed-triple-dotted curve). For southward propagation with winds (long-dashed curve) the variation of the CF with phase speed is less than it is in the windless case. For eastward propagation with winds (solid curve) the undulations in the CF that occur at phase speeds greater than 90 m/s are smaller than those occurring for any of the other cases considered. For the slowest waves (phase speeds $\sim$30 m/s) the mean winds cause the calculated CF's to vary by a factor of $\sim$2 from the CF's calculated without winds. In this case the CF's vary between approximately 0.3 (for northward propagation with winds) and 2.2 (for southward propagation with winds), while the CF's calculated without winds are $\sim$1.0. The differences between the CF's calculated for the different cases considered decrease as the propagation speeds increase from 30 m/s to $\sim$100 m/s. At 100 m/s the CF's all lie between values of about 5 and 7. For the faster gravity waves ($\geq$100 m/s) the CF's display undulations in all cases, with the smallest undulations occurring for both eastward and southward propagation with winds, and the largest undulations occurring for westward and northward propagation with winds. In the most extreme case considered (northward propagation at wave speeds near 175 m/s) the calculated CF's can vary by a factor of $\sim$50 from the CF's calculated without winds. Observations of gravity waves in the airglow rarely, if ever, reveal such fast ($\sim$100 m/s) propagating gravity waves. These, and other considerations to be addressed in the discussion section, suggest that in practice these wind effects occurring at very large phase speeds are unlikely to be ever confirmed by, or relevant to, observations. The reasons for the existence of undulations in the calculated CF's occurring for the faster waves (which are not model artifacts) are explained in detail in the discussion section.

[43] The corresponding results for the case of λ_h = 500 km and winter (15 December) winds (not shown) are different than the λ_h = 100 km case. The cancellation

factor exhibits much less variation with phase speed than in the λ_h = 100 km case (the individual curves are flatter than before) and the strong undulations seen in Figure 8 for the λ_h = 100 km case are replaced by fairly smooth, small amplitude undulations. This difference is primarily due to the fact that for the fast gravity waves the wave periods for λ_h = 500 km are long (several tens of minutes) so that these waves never become evanescent in the thermosphere and so never experience the strong reflections experienced by the fast λ_h = 100 km waves. The effects of mean winds on the cancellation factors are relatively small, and for waves with phase speeds of less than about 100 m/s the winds cause the cancellation factors to vary by no more than about 40%. This is in contrast to the factor of 2 effect of the mean winds noted for the slow λ_h = 100 km gravity waves.

[44] The cancellation factors calculated for summer winds and for λ_h = 100 km (not shown) exhibit large undulations that increase in amplitude with increasing phase speed beyond ~80 m/s, and that are largest for eastward propagation in the presence of winds. Westward propagating gravity waves with phase speeds less than about 65 m/s encounter critical levels below the airglow region (the reverse of what was seen in the winter results), leading to a dramatic increase in the cancellation factors for slower waves which, however, would not be observed in the airglow. For gravity waves with propagation speeds less than about 80 m/s the derived cancellation factors appear far less sensitive to gravity wave propagation direction and winds than in the winter case, and the variation is typically only 50% from the windless case. The cancellation factors calculated for summer winds and for λ_h = 500 km (not shown) exhibit the least sensitivity to the mean winds, and for phase speeds less than about 100 m/s the winds cause the cancellation factors to change by no more than about 20%.

4. Discussion

[45] The altitude distributions of the minor species involved in the airglow emissions vary considerably with location and time, constituting another source of discrepancy between models and measurements. This could be mitigated by using satellite-based measurements of airglow emissions to provide minor species profiles at the approximate time and location of the ground-based measurements, although simultaneous measurements are not always available. The cancellation factors derived from the full-wave and SG98 models are significantly different at long wave periods where chemistry dominates. The SG98 model used simplified chemistry with parameters based on a rather specific set of observations as described by *McDade et al.* [1987]. The full-wave model uses more complete OH chemistry with mean state minor species number densities derived from the MSIS-90 and Garcia-Solomon numerical models [*Hedin*, 1991; *Garcia and Solomon*, 1985]. We expect the latter approach to be more general because it is not tied to any specific observation, but it is also limited by its reliance on model-derived minor species number density profiles. Therefore accurate specification of minor species number density profiles is an essential requirement for model to model and any future model to observation comparisons.

[46] We have considered the linear response of the airglow to gravity waves but 2-D nonlinear modeling studies demonstrate that nonlinear effects can be important at times and drive large secular variations of minor species and the airglow [*Hickey et al.*, 2000b; *Hickey and Walterscheid*, 2001; *Hickey et al.*, 2003; *Xu et al.*, 2003]. The *Swenson and Gardner* [1998] and *Swenson and Liu* [1998] models can allow for a nonlinear gravity wave, but to facilitate comparison with the full-wave model we used small amplitude, linear gravity waves.

[47] The cancellation factor is actually a complex quantity and we have discussed only its amplitude. The phase difference between the gravity wave temperature fluctuation and the airglow brightness fluctuation is also a useful quantity of interest. Difficulties reconciling modeled and measured phase differences between airglow brightness fluctuations and brightness-weighted temperature fluctuations in earlier studies [*Zhang et al.*, 1993a, 1993b] contributed to our understanding of wave ducting in the airglow region [*Hines and Tarasick*, 1994; *Hickey*, 2001a, 2001b]. Coordinated multi-instrumented measurement campaigns could provide the required data, which would then allow more rigorous testing of the models.

[48] The oscillatory behavior of the CF's with increasing phase speed is due to gravity wave reflection occurring from the lower thermosphere. This reflection has two fundamental causes. First, short period (fast) gravity waves can become evanescent as they propagate upward through the lower thermosphere where their period becomes comparable to or less than the local Brunt-Väisälä period. Mean winds will alter where this occurs by changing the intrinsic period of the waves. The mean winds (Figure 7) become quite large in the lower thermosphere, especially so for the meridional winds which reach speeds in excess of ~50 m/s (southward) near 150 km altitude. Therefore upward propagating gravity waves are significantly Doppler shifted at these heights. Waves traveling in a direction opposite to the mean wind (that is, westward or northward for the nominal conditions) will be Doppler shifted to shorter intrinsic periods causing wave reflection to occur sooner (that is, at lower altitudes). Alternatively, gravity waves propagating in the same direction as the mean wind (that is, eastward or southward for the nominal conditions) will be Doppler shifted to longer intrinsic periods causing wave reflection to occur later (that is, at higher altitudes). In this latter case it is possible that the gravity waves may never be reflected if their Doppler shifted (intrinsic) periods remain greater than the local Brunt-Väisälä period.

[49] Second, partial reflections of upward propagating gravity waves can occur if the atmospheric refractive index varies appreciably over a vertical wavelength of a gravity wave, in which case the validity of the WKB approximation becomes questionable. This can occur due to the steep temperature gradient in the lower thermosphere (see Figure 1) and also due to the strong height variation of wave dissipation [*Lindzen*, 1968; *Yanowitch*, 1967, 1969; *Chapman and Lindzen*, 1970]. In both of these cases wave reflection is strongest for the faster gravity waves having large vertical wavelengths. For these waves the atmosphere appears more inhomogeneous [see, e.g., *Einaudi and Hines*, 1971] because the mean state atmospheric refractive index varies significantly over a vertical distance on the order of a

vertical wavelength (and the WKB approximation breaks down).

[50] Here we have compared one numerical model to another in order to compare gravity wave effects in the airglow, but ultimately it is the comparison of model predictions to observations that is of importance. In this respect it is essential that the observations provide the required parameters for meaningful model predictions. Ground-based observations should provide extrinsic wave parameters (wave period, horizontal wavelength, and direction of propagation), mean winds as a function of height, and airglow brightness. The measurements need to be of a high enough sampling frequency and spatial resolution to resolve the waves of interest.

5. Conclusions

[51] Model-derived cancellation factors allow gravity wave amplitudes to be calculated from the amplitude of observed airglow brightness fluctuations. Because gravity wave fluxes of momentum, energy, heat and constituents all depend on the square of wave amplitude, the derived cancellation factors should be determined as completely as possible. For some of the slowest gravity waves considered with phase speeds less than about 40 m s^{-1} derived cancellation factors differed by factors of $\sim$10 between models, implying factors of $\sim$100 between derived gravity wave fluxes of interest. For faster gravity waves with phase speeds greater than $\sim$60 m s^{-1} these model differences became smaller (factors of 2 to 3). We expect the full-wave model to produce better estimates of cancellation factors than the SG98 model only because the full-wave model includes more physical processes. However, our model-to-model comparison needs to be followed by comprehensive model to measurement comparisons in order to determine the limitations associated with both models in their ability to provide agreement with real data. In this respect it is imperative that the major gas amplitude be determined independently of the airglow measurements.

[52] Some of the greatest differences between the cancellation factors derived from the two models occur for slower gravity waves having phase speeds less than about 50 m s^{-1}. These are the same gravity waves that we expect to be most influenced by mean winds. Mean winds are certainly a factor in the determination of wave amplitudes from airglow brightness fluctuations, as previously concluded by *Hickey et al.* [1997, 1998] and *Hickey and Brown* [2002]. Here we find that mean winds are most important for the slower, shorter horizontal wavelength gravity waves. They are also important for the very fast (>100 m/s), short horizontal wavelength gravity waves that become evanescent in the thermosphere and are reflected, but these waves are rarely observed in airglow images.

[53] **Acknowledgments.** This research was supported by NSF grants ATM – 0242889 and ATM – 0242896 to Embry-Riddle Aeronautical University. We thank G. R. Swenson for his useful comments on an earlier version of this manuscript, and Rolando Garcia for kindly providing tables of the undisturbed minor species density profiles.

[54] Arthur Richmond thanks Usama Makhlouf and Gary Swenson for their assistance in evaluating this paper.

References

Booker, J. R., and F. P. Bretherton (1967), The critical layer for internal gravity waves in a shear flow, *J. Fluid Mech.*, *27*, 513.

Bowman, M. R., L. Thomas, and R. H. Thomas (1980), The propagation of gravity waves through a critical layer for conditions of moderate wind shear, *Planet. Space Sci.*, *28*, 119.

Breeding, R. J. (1971), A nonlinear investigation of critical levels for internal atmospheric gravity waves, *J. Fluid Mech.*, *50*, 545.

Chapman, S., and R. S. Lindzen (1970), *Atmospheric Tides*, Springer, New York.

Cowling, D. H., H. D. Webb, and K. C. Yeh (1971), Group rays of internal gravity waves in a wind-stratified atmosphere, *J. Geophys. Res.*, *76*, 213.

Einaudi, F., and C. O. Hines (1971), WKB approximation in application to acoustic-gravity waves, *Can. J. Phys.*, *48*, 1458.

Fritts, D. C. (1984), Gravity wave saturation in the middle atmosphere: A review of theory and observations, *Rev. Geophys.*, *22*, 275.

Garcia, R. R., and S. Solomon (1985), The effects of breaking gravity waves on the dynamics and chemical composition of the mesosphere and lower thermosphere, *J. Geophys. Res.*, *90*, 3850.

Gardner, C. S., and J. D. Shelton (1985), Density response of neutral atmospheric layers to gravity wave perturbations, *J. Geophys. Res.*, *90*, 1745–1754.

Hecht, J. H., T. J. Kane, R. L. Walterscheid, C. S. Gardner, and C. A. Tepley (1993), Simultaneous nightglow and Na lidar observations at Arecibo during the AIDA-89 campaign, *J. Atmos. Sol. Terr. Phys.*, *55*, 409.

Hecht, J. H., R. L. Walterscheid, and M. N. Ross (1994), First measurements of the two-dimensional horizontal wave number spectrum from CCD images of the nightglow, *J. Geophys. Res.*, *99*, 11,449–11,460.

Hecht, J. H., R. L. Walterscheid, M. P. Hickey, and S. J. Franke (2001), Climatology and modeling of quasi-monochromatic atmospheric gravity waves observed over Urbana, Illinois, *J. Geophys. Res.*, *106*, 5181–5195.

Hecht, J. H., R. L. Walterscheid, M. P. Hickey, R. J. Rudy, and A. Z. Liu (2002), An observation of a fast external atmospheric acoustic-gravity wave, *J. Geophys. Res.*, *107*(D20), 4444, doi:10.1029/2001JD001438.

Hedin, A. E. (1991), Extension of the MSIS thermospheric model into the middle and lower atmosphere, *J. Geophys. Res.*, *96*, 1159–1172.

Hedin, A. E., et al. (1996), Empirical wind model for the upper, middle, and lower atmosphere, *J. Atmos. Terr. Phys.*, *58*, 1421.

Hickey, M. P. (1988a), Effects of eddy viscosity and thermal conduction and Coriolis force in the dynamics of gravity wave driven fluctuations in the OH nightglow, *J. Geophys. Res.*, *93*, 4077–4088.

Hickey, M. P. (1988b), Wavelength dependence of eddy dissipation and Coriolis force in the dynamics of gravity wave driven fluctuations in the OH nightglow, *J. Geophys. Res.*, *93*, 4089–4101.

Hickey, M. P. (2001a), Reflection of a long-period gravity wave observed in the nightglow over Arecibo on May 8–9, 1989?, *J. Geophys. Res.*, *106*, 28,199–28,208.

Hickey, M. P. (2001b), Airglow variations associated with nonideal ducting of gravity waves in the lower thermosphere region, *J. Geophys. Res.*, *106*, 17,907–17,917.

Hickey, M. P., and J. S. Brown (2002), A simulation study of space-based observations of gravity waves in the airglow using observed ALOHA-93 wave parameters, *J. Geophys. Res.*, *107*(A12), 1431, doi:10.1029/2001JA009225.

Hickey, M. P., and R. L. Walterscheid (1999), A note on gravity wave–driven volume emission rate weighted temperature perturbations inferred from O_2 atmospheric and OI 5577 airglow observations, *J. Geophys. Res.*, *104*, 4279–4286.

Hickey, M. P., and R. L. Walterscheid (2001), Secular variations of OI 5577 Å airglow in the mesopause region induced by transient gravity wave packets, *Geophys. Res. Lett.*, *28*, 701–704.

Hickey, M. P., R. L. Walterscheid, M. J. Taylor, W. Ward, G. Schubert, Q. Zhou, F. Garcia, M. C. Kelley, and G. G. Shepherd (1997), Numerical simulations of gravity waves imaged over Arecibo during the 10-day 1993 campaign, *J. Geophys. Res.*, *102*, 11,475–11,489.

Hickey, M. P., M. J. Taylor, C. S. Gardner, and C. R. Gibbons (1998), Full-wave modeling of small-scale gravity waves using airborne lidar and observations of the Hawaiian airglow (ALOHA-93) O(^{1}S) images and coincident Na wind, temperature lidar measurements, *J. Geophys. Res.*, *103*, 6439–6453.

Hickey, M. P., R. L. Walterscheid, and G. Schubert (2000a), Gravity wave heating and cooling in Jupiter's thermosphere, *Icarus*, *148*, 266–281.

Hickey, M. P., R. L. Walterscheid, and P. G. Richards (2000b), Secular variations of atomic oxygen in the mesopause region induced by transient gravity wave packets, *Geophys. Res. Lett.*, *27*, 3599.

Hickey, M. P., T.-Y. Huang, and R. L. Walterscheid (2003), Gravity wave packet effects on chemical exothermic heating in the mesopause region, *J. Geophys. Res.*, *108*(A12), 1448, doi:10.1029/2002JA009363.

Hines, C. O. (1960), Internal atmospheric gravity waves at ionospheric heights, *Can. J. Phys.*, *38*, 1441–1481.

Hines, C. O., and C. A. Reddy (1967), On the propagation of atmospheric gravity waves through regions of wind shear, *J. Geophys. Res.*, *72*, 1015.
Hines, C. O., and D. W. Tarasick (1987), On the detection and utilization of gravity waves in airglow studies, *Planet. Space Sci.*, *35*, 851–866.
Hines, C. O., and D. W. Tarasick (1994), Airglow response to vertically standing gravity waves, *Geophys. Res. Lett.*, *21*, 2729.
Holton, J. R. (1982), The role of gravity wave induced drag and diffusion in the momentum budget of the mesosphere, *J. Atmos. Sci.*, *39*, 791.
Huang, T.-Y., M. P. Hickey, T.-F. Tuan, E. Dewan, and R. Picard (2002), Further investigations of the mesospheric inversion layer, *J. Geophys. Res.*, *107*(D19), 4408, doi:10.1029/2001JD001186.
Jones, W. L. (1968), Reflection and stabililty of waves in stably stratified fluids with shear flow, *J. Fluid Mech.*, *34*, 609.
Lindzen, R. S. (1968), Vertically propagating waves in an atmosphere with Newtonian cooling inversely proportional to density, *Can. J. Phys.*, *46*, 1835–1840.
Lindzen, R. S. (1981), Turbulence and stress owing to gravity wave and tidal breakdown, *J. Geophys. Res.*, *86*, 9707.
Liu, A. Z., and C. S. Gardner (2004), Vertical dynamical transport of mesospheric constituents by dissipating gravity waves, *J. Atmos. Sol. Terr. Phys.*, *66*, 267–275.
Liu, A. Z., and G. R. Swenson (2003), A modeling study of O_2 and OH airglow perturbations induced by atmospheric gravity waves, *J. Geophys. Res.*, *108*(D4), 4151, doi:10.1029/2002JD002474.
Makhlouf, U. B., R. H. Picard, and J. R. Winick (1995), Photochemical-dynamical modeling of the measured response of airglow to gravity waves: 1. Basic model for OH airglow, *J. Geophys. Res.*, *100*, 11,289–11,311.
McDade, I. C., E. J. Llewellyn, D. P. Murtagh, and R. G. H. Greer (1987), Eton 5: Simultaneous rocket measurements of the OH Meinel $\Delta\upsilon = 2$ sequence and (8, 3) band emission profiles in the nightglow, *Planet. Space Sci.*, *35*, 1137–1147.
Morton, F. W., and E. A. Essex (1978), Gravity wave observations at a southern hemisphere mid-latitude station using the total electron content technique, *J. Atmos. Terr. Phys.*, *40*, 1113.
Pitteway, M. L. V., and C. O. Hines (1963), The viscous damping of atmospheric gravity waves, *Can. J. Phys.*, *41*, 1935.
Prather, M. J. (1994), Lifetimes and eigenstates in atmospheric chemistry, *Geophys. Res. Lett.*, *21*, 801–804.
Richmond, A. D. (1978), Gravity wave generation, propagation and dissipation in the thermosphere, *J. Geophys. Res.*, *83*, 4131.
Schubert, G., and R. L. Walterscheid (1988), Wave-driven fluctuations in OH nightglow from an extended source region, *J. Geophys. Res.*, *93*, 9903–9915.
Schubert, G., R. L. Walterscheid, and M. P. Hickey (1991), Gravity wave–driven fluctuations in OH nightglow from an extended, dissipative emission region, *J. Geophys. Res.*, *96*, 13,869.
Smith, S. M., M. Mendillo, J. Baumgardner, and R. R. Clark (2000), Gravity wave imaging from a subauroral site: First results from Millstone Hill, *J. Geophys. Res.*, *105*, 27,119–27,130.
Swenson, G. R., and C. S. Gardner (1998), Analytical models for the responses of the mesospheric OH* and Na layers to atmospheric gravity waves, *J. Geophys. Res.*, *103*, 6271–6294.
Swenson, G. R., and A. Z. Liu (1998), A model for calculating acoustic gravity wave energy and momentum flux in the mesosphere from OH airglow, *Geophys. Res. Lett.*, *25*, 477–480.
Swenson, G. R., M. J. Taylor, P. J. Espy, C. S. Gardner, and X. Tao (1995), ALOHA-93 measurements of intrinsic AGW characteristics using the airborne airglow imager and ground-based Na wind/temperature lidar, *Geophys. Res. Lett.*, *22*, 2841–2844.
Swenson, G. R., R. Haque, W. Yang, and C. S. Gardner (1999), Momentum and energy fluxes of monochromatic gravity waves observed by an OH imager at Starfire Optical Range, New Mexico, *J. Geophys. Res.*, *104*, 6067–6080.
Tang, J., A. Z. Liu, and G. R. Swenson (2002), High frequency gravity waves observed in OH airglow at Starfire Optical Range, NM: Seasonal variations in momentum flux, *Geophys. Res. Lett.*, *29*(20), 1966, doi:10.1029/2002GL015794.
Taylor, M. J., E. H. Ryan, T. F. Tuan, and R. Edwards (1993), Evidence of preferred directions for gravity wave propagation due to wind filtering in the middle atmosphere, *J. Geophys. Res.*, *98*, 6047.
Taylor, M. J., M. B. Bishop, and V. Taylor (1995), All-sky measurements of short-period waves imaged in the OI(557.7 nm), Na(589.2 nm), and near-infrared OH and O_2(0, 1) nightglow emissions during the ALOHA-93 campaign, *Geophys. Res. Lett.*, *22*, 2833–2836.
Waldock, J. A., and T. B. Jones (1984), The effects of neutral winds on the propagation of medium-scale atmospheric gravity waves at mid-latitudes, *J. Atmos. Terr. Phys.*, *46*, 217.
Walterscheid, R. L., G. Schubert, and J. M. Straus (1987), A dynamical-chemical model of wave-driven fluctuations in the OH nightglow, *J. Geophys. Res.*, *92*, 1241–1254.
Walterscheid, R. L., J. H. Hecht, R. Vincent, I. M. Reid, J. Woithe, and M. P. Hickey (1999), Analysis and interpretation of airglow and radar observations of quasi-monochromatic gravity waves in the upper mesosphere and lower thermosphere over Adelaide, Australia (35°S, 138°E), *J. Atmos. Sol. Terr. Phys.*, *61*, 461–478.
Xu, J., and A. K. Smith (2003), Perturbations of the sodium layer: Controlled by chemistry or dynamics?, *Geophys. Res. Lett.*, *30*(20), 2056, doi:10.1029/2003GL018040.
Xu, J., A. K. Smith, and R. Ma (2003), A numerical study of the effect of gravity-wave propagation on minor species distributions in the mesopause region, *J. Geophys. Res.*, *108*(D3), 4119, doi:10.1029/2001JD001570.
Yanowitch, M. (1967), Effects of viscosity on gravity waves and the upper boundary condition, *J. Fluid Mech.*, *29*, 209–231.
Yanowitch, M. (1969), A numerical study of vertically propagating waves in a viscous isothermal atmosphere, *J. Comput. Phys.*, *4*, 531–542.
Zhang, S. P., R. N. Peterson, R. H. Wiens, and G. G. Shepherd (1993a), Gravity waves from O_2 nightglow during the AIDA'89 campaign I: Emission rate/temperature observations, *J. Atmos. Terr. Phys.*, *55*, 355–375.
Zhang, S. P., R. H. Wiens, and G. G. Shepherd (1993b), Gravity waves from O_2 nightglow during the AIDA'89 campaign II: Numerical modeling of the emission rate/temperature ratio, η, *J. Atmos. Terr. Phys.*, *55*, 377–395.

M. P. Hickey and Y. Yu, Department of Physical Sciences, Embry-Riddle Aeronautical University, Daytona Beach, FL 32114, USA. (michael.hickey@erau.edu; yonghui.yu@erau.edu)